Synthesis and electrochemical performance of $Ce_{0.05}SnS_2$/graphene nanocomposites as anode materials for lithium-ion batteries

Qiufen Wang[1,2], Ying Huang[1], Juan Miao[2], Wenjing Xu[3]

[1]*The Key Laboratory of Space Applied Physics and Chemistry for the Ministry of Education, School of Science, Northwestern Polytechnical University, Xi'an 710129, People's Republic of China*
[2]*School of Physics and Chemistry, Henan Polytechnic University, Jiaozuo 454000, People's Republic of China*
[3]*Jiaozuo Teachers College, Jiaozuo 454000, People's Republic of China*
E-mail: grp2009waf@163.com

Published in Micro & Nano Letters; Received on 17th May 2014; Revised on 3rd August 2014; Accepted on 11th August 2014

$Ce_{0.05}SnS_2$/graphene (GNS) nanocomposites were synthesised via the hydrothermal method and sintering. The structure and electrochemical performance of the materials were characterised using X-ray diffraction, field emission transmission electron microscopy and electrochemical measurements. The flower-like $Ce_{0.05}SnS_2$ particles with a petal size of 50–100 nm were distributed on graphene sheets. The $Ce_{0.05}SnS_2$/GNS-2 composites exhibited an initial discharge capacity of 1638.3 mAh g^{-1} at 0.5 C, a retention capacity of 707 mAh g^{-1} after 50 cycles, and an improved rate capability because of the support of the nanographene. After their sintering, the $Ce_{0.05}SnS_2$/GNS nanocomposites displayed better electrochemical performance than before sintering.

1. Introduction: Tin-based materials have been used as anode materials for lithium-ion batteries because of their high capacities (>600 mAh g^{-1}) [1–5]. However, the severe volume expansion during the charge–discharge process affects the electrochemical performance. To enhance the electrochemical performance of tin-based materials, compounds such as In–SnS_2 [6] and Ce–Sn [7] are effective materials for accommodating the strain of volume change. Graphene, as a new carbon material, has structural flexibility, high specific surface area and superior electrical conductivity [8]. Sn_3S_4/graphene [9] and SnS_2/grapheme [10–12] nanocomposites are synthesised to improve the reversibility and cycle performance. The availability of graphene effectively alleviates the serious volume expansion of the anode material during intercalation and deintercalation of lithium and creates synergy with active materials that can achieve a higher capacity and improved cycling performance than the materials of Sn_3S_4 and SnS_2.

Based on our previous work on Ce–SnS_2 and graphene-supported Ce–SnS_2 [13, 14], $Ce_{0.05}SnS_2$/GNS nanocomposites have been prepared with the hydrothermal method and sintering as anode materials for lithium-ion batteries.

2. Experiments: Graphene oxide (GO) was synthesised with the modified Hummers and Offeman method [15]. A measure of 2.0 g of natural graphite flakes, 2.0 g of $NaNO_3$, 98 ml of concentrated H_2SO_4 and 12 g of $KMnO_4$ were stirred in a water beaker at 0°C for 1.5 h, and then the solution was stirred at 35°C for 2.5 h, and 80 ml of water was added to the solution at 85°C. Finally, 500 ml of water containing H_2O_2 was added to form the yellow solution. The filtering cake was scattered in water by mechanical agitation. GO sheets were obtained by centrifugation and dried in a vacuum at 60°C.

The content of Ce in the $Ce_{0.05}SnS_2$ nanocomposites was discussed in our previous work [13]. $Ce_{0.05}SnS_2$/GNS nanocomposites were synthesised with the hydrothermal method. A volume of 0.02 mol of $SnCl_4{\cdot}5H_2O$, 0.001 mol of $Ce(NO_3)_3{\cdot}6H_2O$, 0.06 mol of CH_3CSNH_2, 0.5 g of CTAB and 0.24 g of GO were dissolved in alcohol and distilled water. The mixture was moved to an autoclave of 200 ml, and retained at 180°C for 36 h, then left to cool naturally. The solid was dried at 60–70°C to obtain the composites ($Ce_{0.05}SnS_2$/GNS-1). To further reduce graphene, the nanocomposites were sintered at 500°C for 2 h in a tube furnace of Ar to obtain the $Ce_{0.05}SnS_2$/GNS-2 nanocomposites. In addition, $Ce_{0.05}SnS_2$ composites were prepared by the above-mentioned method. Graphene nanosheets (GNSs) were also synthesised by the above-mentioned method by the assistance of CH_3CSNH_2.

The samples were characterised by X-ray diffraction (XRD), scanning electron microscopy (SEM) and a Tecnai F30 G^2 model of transmission electron microscope (TEM). Thermoanalysis of the nanocomposites was performed with the thermogravimetric analysis instrument (TGA, Q50, TA, New Castle DE, USA) in the air atmosphere from 25 to 700 °C.

Electrochemical measurements were evaluated in the system of two electrodes. A lithium metal was used as a counter electrode. The working electrode was prepared by using as-prepared materials of 80 wt%, acetylene black of 10 wt% and PVDF of 10 wt%. The electrolyte was a solution of 1 mol l^{-1} of $LiPF_6$ in the mixture of ethylene (EC), dimethyl carbonate (DMC) and diethyl carbonate (DEC) (1:1:1, v/v/v). The charge and discharge were measured in a battery test system of LAND CT2001A. Electrochemical impedance spectra (EIS) were evaluated on a Redefining Electrochemical Measurement of Series G 750™.

3. Results and discussion: To investigate the content of graphene in the $Ce_{0.05}SnS_2$/GNS-2 nanocomposites, thermogravimetric analysis was made in the air atmosphere from 25 to 700°C. Fig. 1*a* gives the TGA curves of the GNS and $Ce_{0.05}SnS_2$/GNS-2. The curve of the GNS shows a significant weight loss between 400 and 600°C because of the decomposition of the GNS. The curve of $Ce_{0.05}SnS_2$/GNS-2 shows three temperature ranges. The first weight loss between 25 and 200°C may be because of the decomposition of the oxygen-containing group in the graphene. The second between 200 and 380°C may be because of the decomposition of grapheme-to-carbon soot and the oxidation of $Ce_{0.05}SnS_2$ to the oxides of Sn and Ce. The third between 380 and 700°C can be because of the removal of the stable oxygen groups in the graphene and the oxidation of $Ce_{0.05}SnS_2$ into the oxides of Sn and Ce. Thus, the 28.22 wt% weight loss happened between 25 and 700°C. The content of graphene in the $Ce_{0.05}SnS_2$/GNS-2 nanocomposite is estimated to be 23.68 wt%.

The tissue structures for $Ce_{0.05}SnS_2$ have been clarified by XRD and Roman microscopy in our previous work [13]. The surface

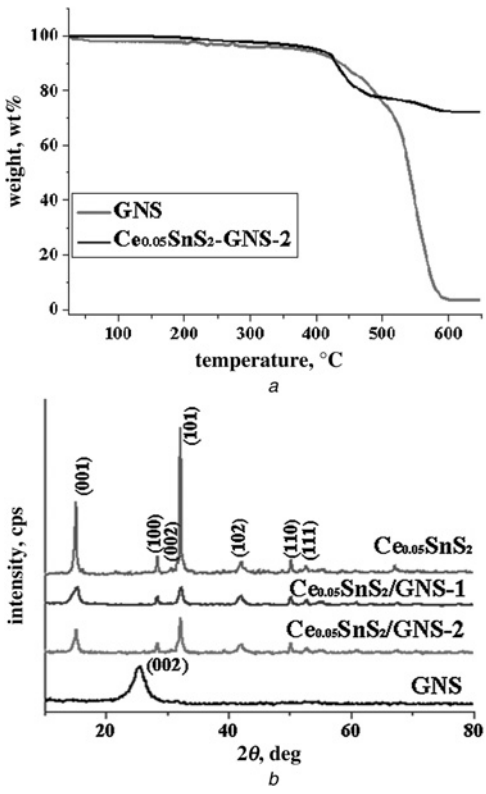

Figure 1 *TGA curves of GNS and $Ce_{0.05}SnS_2$/GNS-2 and XRD patterns of $Ce_{0.05}SnS_2$, $Ce_{0.05}SnS_2$/GNS-1, $Ce_{0.05}SnS_2$/GNS-2 and GNS*
a TGA curves
b XRD patterns

structure and the binding nature of the elements of $Ce_{0.05}SnS_2$ have been further investigated by XPS (seen in [13]). Fig. 1*b* shows the XRD patterns of $Ce_{0.05}SnS_2$, $Ce_{0.05}SnS_2$/GNS-1, $Ce_{0.05}SnS_2$/GNS-2 and GNS. The main diffraction peak of $Ce_{0.05}SnS_2$ agreed with the standard patterns of hexagonal SnS_2 (JCPDS, File No. 23-0677). In the XRD curve of the GNS, the broad peak at $2\theta = 25.8°$ is the plane of (002) in the graphene [16], indicating that there is restacking of multi-graphene layers in the hydrothermal reaction. The main diffraction peaks of the curves of $Ce_{0.05}SnS_2$/GNS-1 and $Ce_{0.05}SnS_2$/GNS-2 are in agreement with those of SnS_2 while their intensity becomes weaker, indicating that the growth of $Ce_{0.05}SnS_2$ crystal particles is inhibited depending on the support of GNS. However, the diffraction peak of the (002) plane in the graphene is not observed, which explains that the stacking in the graphenes is disordered in $Ce_{0.05}SnS_2$/GNS-1 and $Ce_{0.05}SnS_2$/GNS-2 nanocomposites [17]. In addition, the main diffraction peaks of $Ce_{0.05}SnS_2$/GNS-2 are stronger than those of $Ce_{0.05}SnS_2$/GNS-1, indicating that the crystal structure of the nanocomposites becomes more complete after sintering.

Fig. 2 shows the SEM and TEM images of $Ce_{0.05}SnS_2$, $Ce_{0.05}SnS_2$/GNS-1 and $Ce_{0.05}SnS_2$/GNS-2, respectively. Fig. 2*a* reveals that the $Ce_{0.05}SnS_2$ particle has a flower-like structure and is made from several nanopetals with smooth surfaces. For the $Ce_{0.05}SnS_2$/GNS-1 (Fig. 2*b*), the $Ce_{0.05}SnS_2$ particles consist of the agglomerates with an average diameter in the range of 3–5 μm. However, for the $Ce_{0.05}SnS_2$/GNS-2 (Fig. 2*c*), the flower-like $Ce_{0.05}SnS_2$ particle is dispersed randomly on the graphene sheets. The dispersion may help buffer the expansion of the volume of $Ce_{0.05}SnS_2$ particles in the charge and discharge processes [11]. The high-resolution TEM image of $Ce_{0.05}SnS_2$/GNS-2 is shown in Fig. 2*d*. It shows that the flower-like $Ce_{0.05}SnS_2$ particles with a petal size of 50–100 nm are distributed on the wrinkled graphene sheets. The inset shows the selected area electron diffraction (SAED) pattern of $Ce_{0.05}SnS_2$/GNS-2, indicating that the

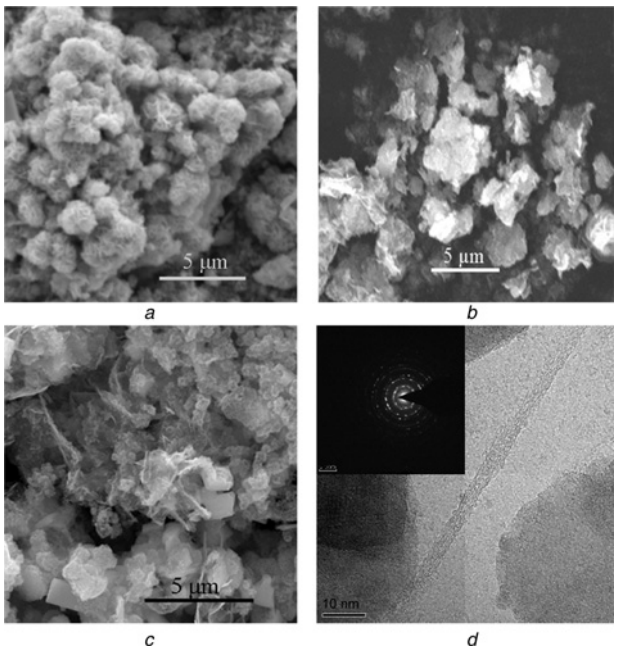

Figure 2 *SEM images and TEM image*
a SEM image of $Ce_{0.05}SnS_2$
b SEM image of $Ce_{0.05}SnS_2$/GNS-1
c SEM image of $Ce_{0.05}SnS_2$/GNS-2
d TEM image of $Ce_{0.05}SnS_2$/GNS-2
Inset is SAED pattern of $Ce_{0.05}SnS_2$/GNS-2

$Ce_{0.05}SnS_2$/GNS-2 nanocomposites have good crystalline characteristics.

Fig. 3*a* shows the first charge–discharge curves of $Ce_{0.05}SnS_2$ $Ce_{0.05}SnS_2$/GNS-1, $Ce_{0.05}SnS_2$/GNS-2 and the GNS at 0.5 C at 0.01–2.0 V against Li^+/Li. The current density is 450 mAg^{-1}. The discharge curves of $Ce_{0.05}SnS_2$/GNS-1 and $Ce_{0.05}SnS_2$/GNS-2 show two potential plateaus at 1.1–1.45 and 0.01–0.5 V, while their charge curves present platforms at 1.5–2.0 and 0.4–0.6 V. The plateau at 1.1–1.45 V can be ascribed to the formation of the solid electrolyte interface film, the reduction of SnS_2 to Sn and the synchronous formation of Li_2S [13, 14]. The plateau (0.01–0.5 V) and the plateau during the charge at 0.4–0.6 V are attributed to the processes of the intercalation and deintercalation of lithium between Li and Sn [11, 13, 14]. The plateau at 1.5–2.0 V may be ascribed to the subsidiary redox reaction between Sn and Li_2S, the Li^+ can intercalate some of itself to the SnS_2 layer without raising the phase decomposition [18]. The initial discharge and charge capacities are 998.2 and 565.4 $mAhg^{-1}$ for $Ce_{0.05}SnS_2$, 1190.6 and 682.0 $mAhg^{-1}$ for $Ce_{0.05}SnS_2$/GNS-1, 1638.3 and 945.9 $mAhg^{-1}$ for $Ce_{0.05}SnS_2$/GNS-2, 1879.2 and 887.3 $mAhg^{-1}$ for GNS, respectively. The discharge and charge capacities of $Ce_{0.05}SnS_2$/GNS-1 and $Ce_{0.05}SnS_2$/GNS-2 are higher than those of $Ce_{0.05}SnS_2$ because of the existence of GNS that has a higher capacity. Moreover, the charge–discharge capacities of $Ce_{0.05}SnS_2$/GNS-2 after sintering are higher than those of $Ce_{0.05}SnS_2$/GNS-1.

Fig. 3*b* shows the cycling curves of the electrodes of $Ce_{0.05}SnS_2$, $Ce_{0.05}SnS_2$/GNS-1, GNS and $Ce_{0.05}SnS_2$/GNS-2 at 0.5 C after 50 cycles between 0.01 and 2.0 V against Li^+/Li. After 50 cycles, the discharge capacity is still 446.2 $mAhg^{-1}$ for $Ce_{0.05}SnS_2$, 570.4 mAh g^{-1} for $Ce_{0.05}SnS_2$/GNS-1, 707.0 mAh g^{-1} for $Ce_{0.05}SnS_2$/GNS-2 and 584.1 mAh $g^{-1}$for GNS, respectively. The improved cyclic ability may be because of the existence of GNS.

Fig. 3*c* shows the rate performance of $Ce_{0.05}SnS_2$ $Ce_{0.05}SnS_2$/GNS-1 and $Ce_{0.05}SnS_2$/GNS-2 after 50 cycles. The cell is first cycled at 0.1 C, then its speeds are turned into 0.3, 0.5, 1.0, 1.5 and 0.1 C, respectively. Obviously, $Ce_{0.05}SnS_2$/GNS-2 presents

doi: 10.1049/mnl.2014.0225

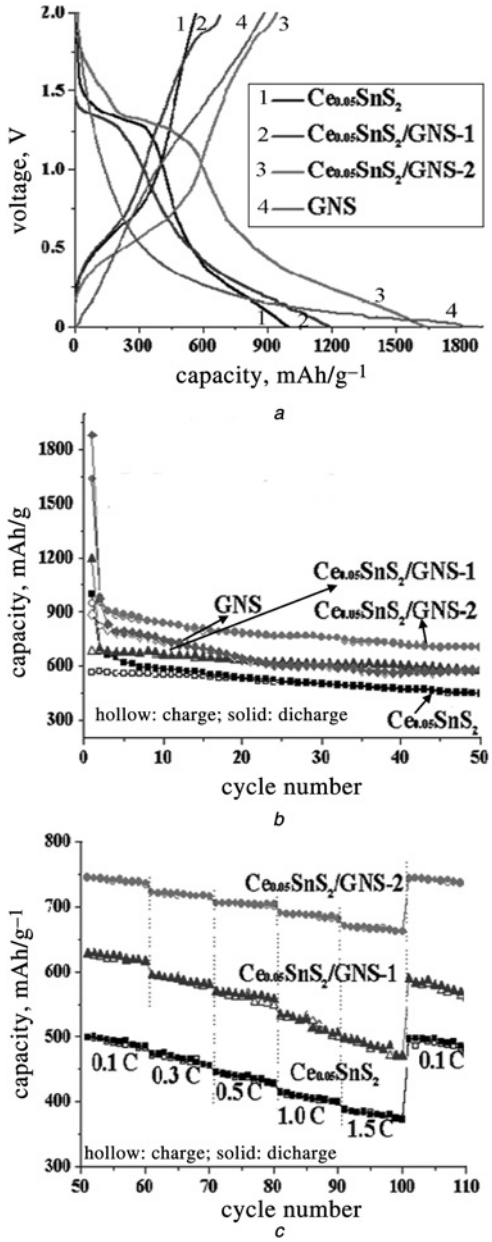

Figure 3 *First charge–discharge curves (Fig. 3a); cycling performances at 0.5 C of $Ce_{0.05}SnS_2$, $Ce_{0.05}SnS_2$/GNS-1, GNS and $Ce_{0.05}SnS_2$/GNS-2 (Fig. 3b); rate performances of $Ce_{0.05}SnS_2$, $Ce_{0.05}SnS_2$/GNS-1 and $Ce_{0.05}SnS_2$/GNS-2 (Fig. 3c)*

the best cycling performance and speed performances in the same conditions. The GNS around $Ce_{0.05}SnS_2$ particles can serve as a buffer matrix to alleviate the expansion of Li–Sn alloy and offer enough ways for the entrance of electrolyte during the discharge and charge processes [19]. Moreover, the electrochemical performance of $Ce_{0.05}SnS_2$/GNS-2 is better than that of $Ce_{0.05}SnS_2$/GNS-1 because the crystallinity of the nanocomposites can be improved after sintering.

Fig. 4 shows the EIS analysis of $Ce_{0.05}SnS_2$ $Ce_{0.05}SnS_2$/GNS-1 and $Ce_{0.05}SnS_2$/GNS-2 at 0.5 V (0.01–100 kHz) after 50 cycles. The equivalent circuit model is shown in the inset of Fig. 4. R_s is ascribed to the electrolyte resistance. R_f is ascribed to the SEI resistance. W is ascribed to the Warburg impedance related to the diffusion of lithium ions into the bulk of the electrode materials. CPE1 and CPE2 are ascribed to two constant phase elements associated with the interfacial resistance and charge-transfer resistance. R_{ct} is ascribed to the charge-transfer resistance [13, 14]. The semi-circle

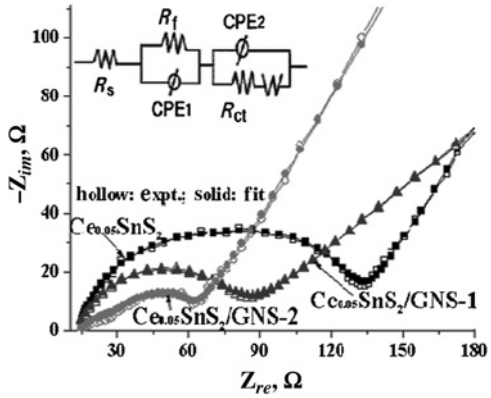

Figure 4 *EIS of $Ce_{0.05}SnS_2$ $Ce_{0.05}SnS_2$/GNS-1 and $Ce_{0.05}SnS_2$/GNS-2 after 50 cycles*
Inset is the equivalent circuit model

of the high frequency is the resistance R_f and CPE1 of the SEI film; the medium-frequency region is because of the charge-transfer resistance R_{ct} and CPE2 of the electrode/electrolyte interface, and the 45° inclined line is because of the lithium-ion diffusion [13, 14]. Obviously, the EIS spectra fitted from the models agree with those of the experiment, suggesting that the equivalent circuit diagram is reasonable. The charge-transfer resistances of $Ce_{0.05}SnS_2$, $Ce_{0.05}SnS_2$/GNS-1 and $Ce_{0.05}SnS_2$/GNS-2 are 132.40, 87.08 and 61.81 Ω, respectively. The high-frequency semicircles and the medium-frequency regions of $Ce_{0.05}SnS_2$/GNS-1 and $Ce_{0.05}SnS_2$/GNS-2 are smaller than those of $Ce_{0.05}SnS_2$ because of the support of the graphene, indicating that the electronic conductivity of $Ce_{0.05}SnS_2$/GNS has been improved after the introduction of GNS. Moreover, the charge-transfer resistance of $Ce_{0.05}SnS_2$/GNS-2 is smaller than that of $Ce_{0.05}SnS_2$/GNS-1, suggesting that the sintering is favourable for the diffusion of lithium ion.

4. Conclusion: $Ce_{0.05}SnS_2$/GNS nanocomposites have been synthesised using the hydrothermal method and sintering. When tests for lithium storage were performed, the $Ce_{0.05}SnS_2$/GNS nanocomposites after sintering showed significantly improved cycling performance compared with the $Ce_{0.05}SnS_2$, which exhibited a high reversibility of 707.0 mAhg^{-1} after 50 cycles, high cyclability and improved rate capability. This method using sintering was demonstrated to be an effective way to improve the cycling performance of the electrode materials.

5. Acknowledgments: This work was supported by the Research Fund for the Doctoral Program of Higher Education of China under Grant no. 20136102110046, the Innovation Foundation of Shanghai Aerospace Science and Technology under Grant no. SAST201373, the Graduate Starting Seed Fund of Northwestern Polytechnical University under fund no. Z2014023, the Basic Research Foundation of Northwestern Polytechnical University under Grant no. JC20126, and Technology Research Project of Jiaozuo Science and Technology Bureau no. 201217.

6 References

[1] Courtney I.A., Dahn J.R.: 'Key factors controlling the reversibility of the reaction of lithium with SnO_2 and Sn_2BPO_6 glass', *J. Electrochem. Soc.*, 1997, **144**, pp. 2943–2948
[2] Du G.D., Guo Z.P., Zhang P., Li Y., Chen M.B., Wexler D., Liu H.K.: 'SnO_2 nanocrystals on self-organized TiO_2 nanotube array as three-dimensional electrode for lithium ion microbatteries', *J. Mater. Chem.*, 2010, **20**, pp. 5689–5694
[3] Wang Q.F., Huang Y., Miao J., Zhao Y., Wang Y.: 'Synthesis and properties of carbon-doped Li_2SnO_3 nanocomposite as cathode material for lithium-ion batteries', *Mater. Lett.*, 2012, **7**, pp. 166–169

[4] Heiba Z.K., Ahmed M.A., Ahmed S.I.: 'Structural investigations of nanomixed oxides SnO_2-xAl_2O_3 prepared by sol-gel technique', *J. Alloys Compd.*, 2010, **507**, pp. 253–256
[5] Wang Q.F., Huang Y., Miao J., Wang Y., Zhao Y.: 'Hydrothermal derived Li_2SnO_3/C composite as negative electrode materials for lithium-ion batteries', *Appl. Surf. Sci.*, 2012, **258**, pp. 6923–6929
[6] Lei Y.Q., Song S.Y., Fan W.Q., Xing Y., Zhang H.J.: 'Facile synthesis and assemblies of flowerlike SnS_2 and In^{3+}-doped SnS_2: hierarchical structures and their enhanced photocatalytic property', *J. Phys. Chem. C*, 2009, **113**, pp. 1280–1285
[7] Sakaguchi H., Honda H., Akasaka Y., Esaka T.: 'Ce–Sn intermetallic compounds as new anode materials for rechargeable lithium batteries', *J. Power Sources*, 2003, **119–121**, pp. 50–55
[8] Novoselov K.S., Geim A.K., Morozov S.V., *ET AL.*: 'Electric field effect in atomically thin carbon films', *Science*, 2004, **306**, pp. 666–669
[9] Yuan C.Z., Hou L.R., Yang L., *ET AL.*: 'Interface-hydrothermal synthesis of Sn_3S_4/graphene sheet composites and their application in electrochemical capacitors', *Mater. Lett.*, 2011, **65**, pp. 374–377
[10] Sathish M., Mitani S., Tomai T., Honma I.: 'Ultrathin SnS_2 nanoparticles on graphene nanosheets: synthesis, characterization, and li-ion storage applications', *J. Phys. Chem. C*, 2012, **116**, pp. 12475–12481
[11] Chang K., Wang Z., Huang G.C., Li H., Chen W.X., Lee J.Y.: 'Few-layer SnS_2/graphene hybrid with exceptional electrochemical performance as lithium-ion battery anode', *J. Power Sources*, 2012, **201**, pp. 259–266
[12] Zhong H.X., Yang G.Z., Song H.Z., *ET AL.*: 'Vertically aligned graphene-like SnS_2 ultrathin nanosheet arrays: excellent energy storage, catalysis, photoconduction, and field-emitting performances', *J. Phys. Chem. C*, 2012, **116**, pp. 9319–9326
[13] Wang Q.F., Huang Y., Miao J., Zhao Y., Wang Y.: 'Synthesis and electrochemical characterizations of Ce doped SnS_2 anode materials for rechargeable lithium ion batteries', *Electrochim. Acta*, 2013, **93**, pp. 120–130
[14] Wang Q.F., Huang Y., Miao J., Zhao Y., Zhang W., Wang Y.: 'Graphene-supported Ce–SnS_2 nanocomposite as anode material for lithium-ion batteries', *J. Am. Ceram. Soc.*, 2013, **96**, pp. 2190–2196
[15] Hummers W.S., Offeman R.E.: 'Preparation of graphitic oxide', *J. Am. Chem. Soc.*, 1958, **80**, p. 1339
[16] Nethravathi C., Rajamathi M.: 'Chemically modified graphene sheets produced by the solvothermal reduction of colloidal dispersions of graphite oxide', *Carbon*, 2008, **46**, pp. 1994–1998
[17] Zhang J.T., Xiong Z.G., Zhao X.S.: 'Graphene-metal-oxide composites for the degradation of dyes under visible light irradiation', *J. Mater. Chem.*, 2011, **21**, pp. 3634–3640
[18] Connor P.A., Irvine J.T.S.: 'Novel tin oxide spinel-based anodes for Li-ion batteries', *J. Power Sources*, 2001, **97–98**, pp. 223–225
[19] Sharma N., Shaju K.M., Subba Rao G.V., Chowdari B.V.R.: 'Anodic behavior and X-ray photoelectron spectroscopy of ternary tin oxides', *J. Power Sources*, 2005, **139**, pp. 250–260

doi: 10.1049/mnl.2014.0225